HIV-1 Rev protein assembles on viral RNA one molecule at a time

Stephanie J. K. Pond, William K. Ridgeway, Rae Robertson, Jun Wang, and David P. Millar[1]

Department of Molecular Biology, The Scripps Research Institute, La Jolla, CA 92037

Edited by Ignacio Tinoco, Jr., University of California, Berkeley, CA, and approved December 5, 2008 (received for review July 29, 2008)

Oligomerization of the HIV-1 protein Rev on the Rev Response Element (RRE) regulates nuclear export of genomic viral RNA and partially spliced viral mRNAs encoding for structural proteins. Single-molecule fluorescence spectroscopy has been used to dissect the multistep assembly pathway of this essential ribonucleoprotein, revealing dynamic intermediates and the mechanism of assembly. Assembly is initiated by binding of Rev to a high-affinity site in stem-loop IIB of the RRE and proceeds rapidly by addition of single Rev monomers, facilitated by cooperative Rev-Rev interactions on the RRE. Dwell-time analysis of fluorescence trajectories recorded during individual Rev-RRE assembly reactions has revealed the microscopic rate constants for several of the Rev monomer binding and dissociation steps. The high-affinity binding of multiple Rev monomers to the RRE is achieved on a much faster timescale than reported in previous bulk kinetic studies of Rev-RRE association, indicating that oligomerization is an early step in complex assembly.

ribonucleoprotein assembly | single-molecule fluorescence spectroscopy | viral RNA trafficking

Rev, a key regulatory protein of HIV-1, activates nuclear export of unspliced and partially spliced viral mRNAs, encoding genomic RNA and the structural proteins Gag, Pol, and Env, respectively (reviewed in ref. 1). Rev binds to a highly conserved region of the viral mRNA known as the Rev Response Element (RRE). The RRE contains a single high-affinity binding site for Rev, although as many as 8 Rev molecules can bind to a single RNA (2–4). In fact, binding of a single Rev molecule to the RRE is incapable of activating mRNA export, indicating that oligomerization of Rev on the RRE is required for Rev function (5, 6). Because Rev-mediated RNA export is essential for viral replication, the Rev-RRE complex is a potential therapeutic target for treatment of HIV/AIDS, although effective inhibitors of Rev function have yet to be developed.

Despite the important role of the Rev-RRE ribonucleoprotein (RNP) in the HIV-1 life cycle, the mechanism of oligomeric complex assembly is not well understood. Previous studies have suggested that a single Rev monomer initially binds to the high-affinity site, after which additional monomers assemble on adjacent regions of the RRE (3, 6, 7). Alternatively, preformed oligomers of Rev might bind directly to the RRE (8, 9), because Rev is known to self-associate in the absence of RNA, with an association constant of $1 \times 10^6\ M^{-1}$ (10). To date, it has not been possible to distinguish these assembly models, because all previous studies have been performed under ensemble-averaged conditions at relatively high protein concentrations. Here, we use single-molecule fluorescence spectroscopy to observe individual steps of RNP assembly. Our results clearly demonstrate that multiple Rev monomers bind sequentially to the RRE and they establish a detailed kinetic framework for the early steps of Rev-RRE assembly. Moreover, the method described here could be used to visualize the dynamic assembly of other biologically important RNPs.

Results

A truncated RRE construct, corresponding to approximately half of the full-length RRE, was immobilized by biotin/streptavidin interactions on a quartz slide in the sample chamber of a wide field total internal reflection fluorescence (TIRF) microscope. The construct contains the high-affinity Rev binding site in stem-loop IIB, and each of the other stems of the RRE, but is truncated within stem I (Fig. 1*A*). Based on previous biochemical analyses of similar truncated RRE variants, this construct is expected to bind up to 4 Rev monomers (4, 7), which was confirmed here by a gel electrophoretic titration (data not shown). To detect binding events at the single-molecule level, Rev was specifically labeled at a single cysteine residue with the bright fluorescent dye Alexa Fluor 555 (A555). TIRF microscopy (11) was used to observe individual Rev molecules as they bound to and dissociated from the immobilized RRE molecules. The surface was coated with polyethylene glycol (PEG) blocking groups to suppress nonspecific adsorption of Rev (12). For these measurements, the labeled Rev was supplied at a concentration of 1 nM.

Typical fluorescence intensity trajectories (time traces) reveal discrete and abrupt transitions between states exhibiting different fluorescence intensity (Fig. 2*A*), reflecting individual binding and dissociation events. The specificity of the Rev-RRE interaction was tested by using a PEG-treated surface lacking any attached RRE molecules. Intensity trajectories recorded under the same conditions revealed only a few Rev binding and dissociation events, which together account for $<10\%$ of the number of events observed when the RRE was immobilized on the surface. Hence, the majority of transitions observed with the RRE present on the surface represent Rev-RRE binding and dissociation events. The signal arising from free Rev molecules diffusing in bulk solution was also negligible, because the background intensity levels measured with or without 1 nM Rev in the sample cell were identical.

The intensity histogram compiled from $\approx$1,000 trajectories of individual Rev-RRE complexes shows 4 distinct bound states, with evenly spaced fluorescence intensities, which we interpret as stepwise increasing Rev:RRE stoichiometries (Fig. 2*A*). Similar measurements performed with the V16D/I55N Rev mutant revealed only the lowest intensity state (Fig. 2*B*). Because the V16D/I55N mutations are known to block oligomerization of Rev on the RRE (13), the lowest intensity state is assigned to the 1:1 Rev-RRE complex. Given their relative emission intensities, the remaining states observed in Fig. 2*A* (in order of increasing brightness) are assigned to 2:1, 3:1, and 4:1 complexes.

In the trajectory shown in Fig. 2*A*, the intensity jumps occur in steps of ± 1 Rev monomer, consistent with a sequential monomer binding pathway of complex assembly. To test the

Author contributions: D.P.M. designed research; S.J.K.P. and R.R. performed research; S.J.K.P., W.K.R., and J.W. contributed new reagents/analytic tools; S.J.K.P., R.R., and D.P.M. analyzed data; and S.J.K.P., W.K.R., and D.P.M. wrote the paper.

The authors declare no conflict of interest.

This article is a PNAS Direct Submission.

[1]To whom correspondence should be addressed. E-mail: millar@scripps.edu.

This article contains supporting information online at www.pnas.org/cgi/content/full/0807388106/DCSupplemental.

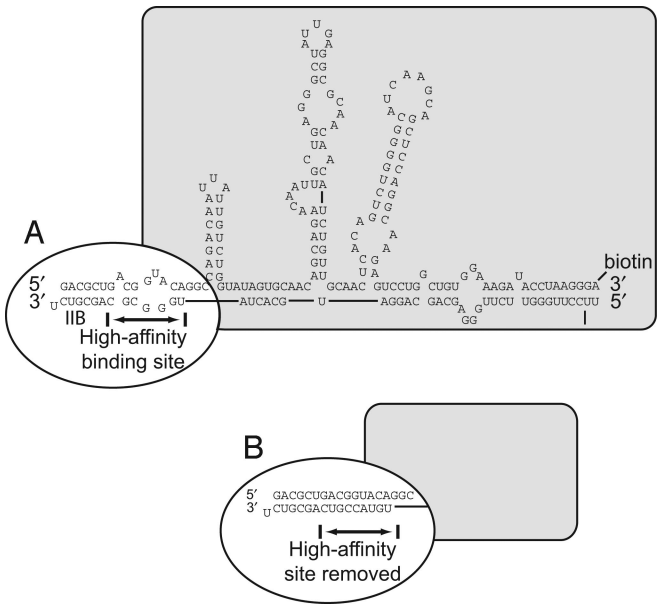

Fig. 1. Sequence and secondary structure of the RRE construct used in the present study. Stem I and stem-loop IIB are labeled with Roman numerals. (*A*) Construct containing the high-affinity Rev binding site in stem-loop IIB. (*B*) Construct lacking the high-affinity binding site, with fully complementary duplex RNA in stem IIB. The gray box symbolizes the remainder of the RRE construct, which is identical to the corresponding boxed area in *A*.

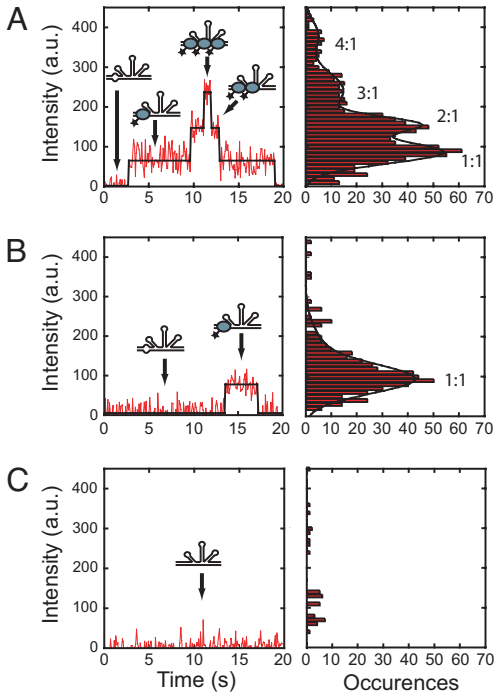

Fig. 2. Rev-RRE complex assembly observed by single-molecule TIRF microscopy. (*A*) Representative fluorescence intensity trajectory for a single complex of Rev and RRE is shown at left (red), together with the mean intensity during each dwell period (black lines). The fluorescence intensity histogram compiled from ≈1,000 such trajectories is shown on the right (red) and is fit to 4 Gaussian peaks (black lines), corresponding to stepwise increasing Rev:RRE stoichiometries. The peak corresponding to the background intensity is not shown for clarity. (*B*) Representative intensity trajectory and intensity histogram obtained with an oligomerization-deficient V16D/I55N Rev mutant (13). Only one state is sampled in the representative trajectory (*Left*) and only a single population appears in the intensity histogram (*Right*). The mean intensity is equivalent to the 1:1 stoichiometry state in *A*. (*C*) Rev is added to a modified RRE construct in which the high-affinity Rev binding site in stem-loop IIB is replaced by duplex RNA (construct shown in Fig. 1*B*). No binding or dissociation events are observed.

generality of this observation, we compiled the distribution of intensity jump sizes for 16,458 transitions (Fig. 3). More than 90% of transitions fall within the range expected for binding or dissociation of a single Rev monomer. Hence, sequential monomer binding is the predominant mode of Rev-RRE complex assembly.

Previous studies suggest that the first Rev monomer binds to the high-affinity site, located within the internal loop of stem IIB of the RRE (4, 7). To test the role of the high-affinity site in complex assembly, the internal loop was substituted with fully complementary duplex RNA (Fig. 1*B*). This modification of the RRE eliminated all binding events (Fig. 2*C*), confirming that oligomeric assembly is indeed nucleated by the binding of a Rev monomer to the high-affinity site. This result further indicates that Rev has a low intrinsic affinity for secondary sites in the RRE under the present experimental conditions, suggesting that higher-order complex formation is driven primarily by protein–protein interactions.

Kinetic information on the Rev binding and dissociation steps was obtained by compiling the distribution of dwell times for each stoichiometry state before an upward or downward intensity transition (examples of dwell-time histograms are shown in supporting information (SI) Fig. S1 and Fig. S2). The resulting histograms were fitted with exponential functions in order to determine the corresponding rate constants (summarized in Fig. 4). Apart from the first Rev binding transition, the dwell-time histograms for the binding and dissociation steps (Fig. S2) are adequately fitted with a single exponential decay (R^2 values in the range 0.85–0.92), and the fits are not significantly improved by the inclusion of a second exponential or a constant background term. In contrast, the dwell-time histogram for the initial Rev binding transition (Fig. S1) is fitted better with a double exponential ($R^2 = 0.92$) than a single exponential ($R^2 = 0.78$). The fast phase, accounting for 75 ± 15% of the total events, has an apparent rate of 0.53 ± 0.17 s^{-1}, corresponding to a bimolecular association rate constant of $5.3 \pm 1.7 \times 10^8$ $M^{-1}s^{-1}$ at the Rev concentration used (1 nM). This value is comparable to the diffusional encounter rate of two small proteins in solution (14). The slow phase has a rate of 0.040 ± 0.015 s^{-1}, corresponding to a bimolecular rate constant of $4.0 \pm 1.5 \times 10^7$ $M^{-1}s^{-1}$. This phase may arise from a minor population of RRE molecules that bind Rev more slowly. Note that only the fast association rate (major component) is shown in Fig. 4. The second, third, and fourth Rev monomers also bind rapidly to the RRE with bimolecular rate constants in a similar range and with a single kinetic phase (Fig. 4). Each of the Rev monomers dissociates from the RRE at a similar rate (0.14–0.22 s^{-1}; Fig. 4) and only a single kinetic phase is observed in each case.

In principle, photobleaching of the A555 dye could be responsible for some of the downward intensity transitions, despite the presence of the oxygen scavenger propyl gallate in the surrounding solution. To assess the possible influence of dye photobleaching, we repeated the TIRF measurements across a range of laser excitation powers from 40 to 70 mW. The rate of dye photobleaching is expected to increase with the excitation intensity. However, we did not observe any significant change in the apparent rates of the Rev dissociation steps across this range of laser powers. In addition, we directly measured the dye photobleaching rate under identical experimental conditions by using an immobilized RNA construct labeled with Alexa Fluor 555. The dye photobleaches at a rate 8.5 ± 0.1 × 10^{-3} s^{-1} under the illumination conditions used in the TIRF measurements of the

BIOPHYSICS

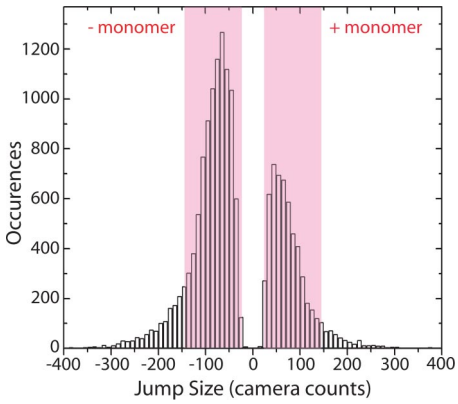

Fig. 3. Assembly and dissociation of oligomeric Rev-RRE complexes occur in steps of a single Rev monomer. The distribution of jump sizes obtained from analysis of 16,458 fluorescence intensity transitions is shown. The positive jumps correspond to Rev binding events, whereas the negative jumps correspond to Rev dissociation or dye photobleaching events. The shaded regions correspond to the range of jump sizes expected for binding or dissociation of a single Rev monomer under the experimental conditions, extending from $\mu - 2\sigma$ to $\mu + 2\sigma$, where μ and σ are the mean and standard deviation, respectively, of the Gaussian fit to the 1:1 intensity peak in Fig. 2*A*. More than 94% of upward transitions and 91% of downward transitions fall within the expected monomer intensity intervals.

Rev-RRE system, substantially slower than any of the Rev dissociation steps (Fig. 4). Note that the dissociation rates shown in Fig. 4 are corrected for the small contribution of dye photobleaching, through the use of Eq. **2**.

The association and dissociation rates recovered from dwell-time analysis were used to calculate the equilibrium dissociation constants for each step of Rev-RRE complex assembly, and the resulting values are presented at the bottom of Fig. 4. Clearly, each of the Rev monomers is bound tightly to the RRE. Notably, the K_D values determined from our kinetic data are consistent with reported bulk values of 0.3–2 nM for Rev and full-length RRE (2, 10, 15), considering that the bulk values are an average over all protein binding events. Moreover, this agreement confirms that the presence of the A555 dye label in our Rev construct does not appreciably alter the affinity of Rev for the RRE.

Discussion

The interaction of Rev with the RRE is a complex process. Despite harboring just a single high-affinity binding site, the full RRE can bind as many as 8 Rev molecules (2–4). In fact, oligomerization of Rev on the RRE is essential for Rev function, because the 1:1 Rev:RRE complex does not promote nuclear export of RRE-containing mRNA (5, 6). Individual RNP complexes with different Rev:RNA stoichiometries can be readily resolved by gel electrophoresis, as reported by several groups (3, 4, 6, 15, 16). Despite the experimental consensus, these observations have been interpreted in 2 different ways. In one proposed model, a single Rev monomer nucleates assembly by binding to the high-affinity site in stem-loop IIB, after which additional monomers bind sequentially to adjacent sites on the RRE (3, 17), most likely along stem I (4). Alternatively, it was proposed that Rev must oligomerize in solution before binding to the RRE (8, 9). The latter model is supported by the observation that Rev can self-associate in solution to form a distribution of oligomeric species (10). It is important to emphasize that these 2 assembly models cannot be distinguished from measurements of the equilibrium distribution of the various Rev-RRE complexes, as reported by gel electrophoresis or other static methods.

To overcome this limitation, we have devised a single-molecule fluorescence spectroscopic method to observe the dynamic assembly of fluorophore-labeled Rev on a single immobilized RRE molecule in real time. The fluorescence intensities measured with this system are quantized into 4 evenly spaced levels, consistent with the expected binding of up to 4 Rev molecules to the truncated RRE construct. Moreover, only the lowest intensity level is observed when the V16D/I55N Rev mutant is used, which is known to arrest assembly at the 1:1 Rev-RRE complex (13). Mutation of the high-affinity binding site in stem-loop IIB of the RRE eliminates all intensity states, consistent with the critical role of this site in nucleating the oligomeric assembly of Rev on the RRE. Taken together, these results establish that the different intensity levels represent individual Rev-RRE complexes with stepwise increasing stoichiometry. The fluorescence intensities scale linearly with the number of bound Rev monomers, indicating that there is negligible self-quenching, despite the presence of multiple dye molecules within the higher-order complexes. Hence, the single-molecule fluorescence system is well behaved and reproduces known properties of the Rev-RRE system.

This new experimental system has allowed us to discriminate between the 2 previously proposed models for Rev-RRE complex assembly. By monitoring the fluorescence intensity over time, we have counted the number of labeled Rev molecules that associate with the RRE during each step of assembly. Moreover, because binding is reversible, we also observe spontaneous dissociation events in the fluorescence trajectories. The majority of the observed intensity jumps (>90%) fall within the range expected for a single Rev molecule, demonstrating that Rev monomers bind to and dissociate from the RRE one at a time. These results constitute the first definitive evidence for the sequential monomer binding model of Rev-RRE complex assembly.

It is formally possible that 2 Rev molecules bind simultaneously to the RRE, one of which has photobleached before binding. Such an event would be falsely registered as a monomer binding event. Based on the measured rate of photobleaching, ≈15% of Rev molecules could photobleach during a 20-s data acquisition, provided they remained in the evanescent field (≈100 nm deep) for the entire time before binding to the RRE. However, because the Rev molecules are not tethered, they are free to diffuse in and out of the evanescent field and to exchange with the vast excess of unbleached Rev molecules in bulk solution (≈500-fold excess, based on the relative dimensions of the

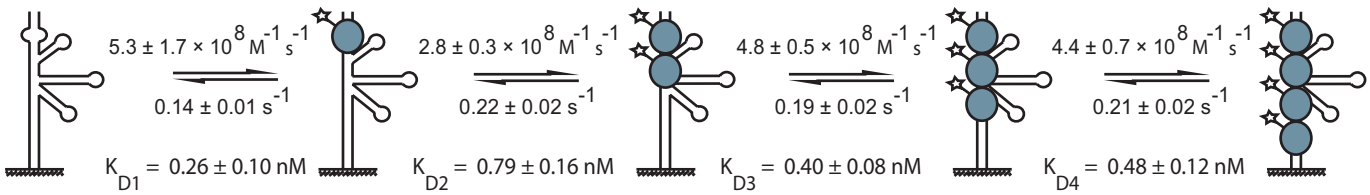

Fig. 4. Summary of sequential association and dissociation rates for Rev-RRE complex assembly, compiled from an analysis of 16,458 transitions. The corresponding equilibrium dissociation constants for each step in the assembly pathway are shown at the bottom of the figure.

evanescent illumination zone and the sample cell). Hence, the fraction of prebleached Rev molecules that bind to the RRE is expected to be inconsequentially small.

Oligomerization of Rev on the RRE appears to be a highly cooperative process. The first Rev monomer binds the RRE with high affinity ($K_D = 0.26 \pm 0.09$ nM), reflecting the formation of a specific RNA–protein interface. This interaction requires the presence of the internal loop in stem IIB, consistent with previous studies showing that the high-affinity Rev binding site is localized in this region of the RRE (7, 15). The second Rev monomer also binds the RRE with high affinity ($K_D = 0.77 \pm 0.13$ nM), provided that the nucleating Rev monomer is also present. However, if the nucleating monomer is absent, by removal of the internal loop in stem IIB, no significant Rev binding events are observed, indicating that Rev has a low intrinsic affinity for the flanking RNA. We estimate the K_D value for the nonspecific Rev–RNA interaction must exceed 100 nM, because any dissociation constant smaller than this value would have produced a detectable level of binding under the conditions of our experiments. Hence, the second Rev monomer is bound at least 130-fold more tightly when the nucleating monomer is also present, indicating a high degree of thermodynamic cooperativity in the binding of these monomers. Presumably, the cooperativity arises from protein–protein interactions between adjacent Rev monomers. These cooperative protein–protein interactions are disrupted by the V16D/I55N Rev mutations, suggesting that Val-16 and/or Ile-55 are located at the monomer–monomer interface, consistent with the assembly model proposed by Jain and Belasco (17). The third and fourth Rev monomers are also bound more tightly than expected from protein–RNA interactions alone (Fig. 4), indicating that these Rev molecules also participate in cooperative protein–protein interactions on the RRE.

Dwell-time analysis of the intensity trajectories has provided detailed kinetic information on each of the association and dissociation steps during Rev-RRE complex assembly. Each of the Rev monomers binds rapidly to the RRE, with bimolecular rate constants (Fig. 4) that are comparable to the diffusional encounter rate of 2 small proteins in solution (14). The rapid association might be aided by electrostatic attraction between the negatively charged RNA backbone and the 10 positively charged arginine residues within the RNA binding domain of Rev. In favorable circumstances, electrostatic attraction can accelerate bimolecular association by a factor of up to 10^3-10^4 compared with the rate of translational diffusion alone (14, 18). However, it is important to emphasize that the single-molecule experiments are not simply reporting the formation of diffusional encounter complexes, because the binding events depend on the presence of the internal loop in stem IIB (Fig. 2*C*), indicating an ordered rather than stochastic assembly process, and the calculated dissociation constants are in the low to subnanomolar range, reflecting high-affinity interactions (Fig. 4). The dwell-time histogram for the first association step also reveals a slower kinetic phase that is not apparent during any of the subsequent Rev binding steps. Hence, this phase may arise from a minor population of misfolded RRE molecules that bind the first Rev monomer slowly and are incapable of progressing beyond the 1:1 complex.

The association rates obtained from our TIRF measurements are 2–3 orders of magnitude faster than those reported in previous bulk surface plasmon resonance (SPR) experiments that also utilized an immobilized RRE molecule (19), even allowing for the slow kinetic phase observed during binding of the first Rev monomer. This discrepancy could be due to differences in assay format, experimental conditions, and the materials used in each case. Moreover, the physical basis for the 2 assays is fundamentally different. The SPR experiments monitor the progressive accumulation of many Rev molecules on the sensor chip, whereas our TIRF experiments monitor the rapid and reversible binding of individual Rev monomers during the early stages of complex assembly.

The single-molecule TIRF measurements reported here have established the basic mechanism of Rev-RRE complex assembly. Assembly of the Rev-RRE complex within the nucleus of a HIV-1-infected human cell occurs in the presence of many host proteins. In fact, a variety of nuclear proteins are known to associate with the Rev-RRE complex and are essential for Rev function, such as the nuclear export receptor CRM1 (20) and the DEAD box protein DDX1 (21). These and other proteins could potentially influence how Rev interacts with the RRE or they might stabilize Rev-RRE complexes once formed. Future studies will pursue the goal of creating RNPs that better resemble export-competent complexes, by addition of selected cellular cofactors to the Rev-RRE assembly reactions. The present study of the binary Rev-RRE system establishes an important first step in elucidating the assembly pathway of the RNPs involved in viral RNA trafficking. More generally, the degree of information provided by the single-molecule assay constitutes a technological advance in our capabilities to study macromolecular complex assembly and we anticipate its utility in a variety of systems.

Materials and Methods

RRE Constructs. The RRE construct used in most of the experiments is formed from 2 RNA strands, a synthetic 48-mer and an in vitro transcribed 161-mer (Fig. 1*A*). The synthetic RNA strand, RRE_{48}, with the sequence (5′ to 3′) UUC CUU GGG UUC UUG GGA GCA GCA GGA XGC ACU AUG GGC GCA GCG UCU-$(CH_2)_3$-SH, where X is NH_2-$(CH_2)_6$-dU, was obtained from Eurogentech S.A., and was PAGE purified. The second strand for the RRE construct, RRE_{161}, was generated by in vitro transcription and subsequently biotinylated at the 3′ end for surface attachment (*SI Text*). RRE_{48} and biotinylated RRE_{161} were annealed in 20 mM Hepes (pH 7.5), 140 mM NaCl, 10 mM $MgCl_2$, and 10 mM DTT at 95 °C for 5 min and then slowly cooled to 4 °C. This procedure yields a single annealing product, evident in a 10% native polyacrylamide gel (data not shown). A second RRE construct was formed by annealing the biotinylated RRE_{161} with a different synthetic oligonucleotide, RRE_{50}, with the following sequence (5′ to 3′) UUC CUU GGG UUC UUG GGA GCA GCA GGA UGC ACU AUG UAC CGU CAG CGU CU. This construct replaces stem-loop IIB with fully complementary duplex RNA (Fig. 1*B*).

Rev Proteins. Purified recombinant Rev proteins were based on the sequence MGHHHH $^{-10}$HHSSGLFKRH ^{0}MAGRSGDSDE ^{10}DLLKAVRLIK ^{20}FLYQSNPPPN ^{30}PEGTRQARRN ^{40}RRRRWRERQR ^{50}QIHSISERIL ^{60}STYLGRSAEP ^{70}VPLQLPPLER ^{80}LTLDCNEDCG ^{90}TSGTQGVGSP ^{100}QILVESPTVL ^{110}ESGTKE were a gift from the laboratory of James R. Williamson (Scripps Research Institute). In the numbering system, the sequence of wt Rev begins at residue zero. The N-terminal extension (residues −1 to −16) contains a hexahistidine tag used for affinity purification. One construct was mutated (C85S, site indicated in bold type above) such that there is only a single cysteine residue present at position 89 available for fluorophore labeling. For simplicity, this construct is referred to as Rev. Cys-85 and Cys-89 are both well removed from the RNA binding region of Rev (amino acids 34–50), such that mutation of one of the cysteines and labeling of the other is not expected to impair the RNA binding activity of the protein. An oligomerization-deficient Rev mutant contained V16D and I55N mutations (13) (sites also indicated in bold above), in addition to the C85S mutation and N-terminal extension. This construct is referred to as V16D/I55N Rev. Both Rev constructs were covalently labeled with Alexa Fluor555 at the single cysteine, resulting in >90% labeling as determined by MALDI mass spectrometry. The labeled and unlabeled Rev proteins were separated by HPLC purification under denaturing conditions (the 2 species were completely resolved with baseline separation), affording 100% labeled material. Labeled Rev constructs were refolded by equilibrium dialysis, aliquoted and stored at −80 °C before measurement (*SI Text*).

Total Internal Reflection Fluorescence Microscopy. Measurements were performed by using a custom-built, prism-based total internal reflection fluorescence microscope. A tunable argon-ion laser set to 514 nm and 40–70 mW average power (Melles-Griot) was directed through a beam expander and focused onto a quartz prism in contact with a sample chamber mounted on the stage of an inverted Axiovert 200 microscope (Zeiss). The laser beam entered the prism at an angle of 70°, above the critical angle required for total internal

reflection. The prism was in contact (via a glycerol layer) with a refractive index matched quartz slide, which had been treated with polyethylene glycol to minimize nonspecific protein adsorption and with streptavidin for surface attachment of the sample (*SI Text*). The sample consists of 100 pM biotinylated RRE and 1 nM Rev-A555 in 10 mM Hepes (pH 7.5), 150 mM KCl, 10 mM K_2SO_4, 2 mM $MgCl_2$, and 2 mM DTT. The sample was preincubated for 5 min, 1 mM propyl gallate was added as an oxygen scavenger, and the resulting mixture was flowed into the sample chamber before measurements. The sample fluorescence was collected by using a Plan Apo 63 × 1.2 NA extra-long working distance water-immersion objective (Zeiss), and separated from the scattered excitation light with a dichroic mirror (z514rdc, Chroma) and bandpass filter (HQ530lp, Chroma). The fluorescence passed through a 630dcxr dichroic mirror and HQ585/60 bandpass filter (Chroma) and detected by a cooled intensified CCD camera (I-PentaMAX, Princeton Instruments) with an integration time of 100 ms per frame.

TIRF Data Analysis. Fluorescence intensity trajectories (time traces) of individual Rev-RRE complexes were extracted from raw CCD camera movie files by using a custom-written script (*SI Text*). The trajectories were analyzed by hidden Markov analysis by using the program HAMMY[22], to construct intensity histograms and determine the number of distinct intensity states. A custom program was used to identify the transition points between distinct intensity states, yielding the dwell time for each state sampled in the trajectory. These values were used to construct dwell-time histograms by using Origin software. The dwell-time histograms for upward intensity transitions were fit to a single- or double-exponential function, according to Eq. **1**:

$$N(t) = \sum_i A_i \exp(-k_{\mathrm{on},i}t) \qquad [1]$$

where $N(t)$ is the number of occurrences of dwell time t, A_i is an amplitude factor, $k_{\mathrm{on},i}$ is the first-order rate constant for component i and $i = 1$ or 2. The corresponding bimolecular rate of association, $k_{\mathrm{ass},i}$, was calculated as $k_{\mathrm{ass,i}} = k_{on,i}/[\mathrm{Rev}]$, where [Rev] is the free Rev concentration. Because Rev was present in excess relative to the RRE, the free Rev concentration was well approximated by the total Rev concentration. The dwell-time histograms for downward intensity transitions were fit to a single- or double-exponential function, with separate rate terms for Rev dissociation and photobleaching of the Alexa Fluor 555 dye,

$$N(t) = \sum_i A_i \exp(-[k_{\mathrm{diss},i} + k_{\mathrm{pb}}]t) \qquad [2]$$

where $k_{\mathrm{diss},i}$ is the dissociation rate for component i ($i = 1$ or 2) and k_{pb} is the rate of dye photobleaching. A correlation coefficient (R^2 value) was calculated in every case to determine whether the dwell-time histograms were best represented by single- or double-exponential functions.

Dye Photobleaching Kinetics. An RNA duplex corresponding to stem IIB of the RRE was formed from 2 RNA oligonucleotides. One strand was labeled at the 3′ end with Alexa Fluor 555 and at the 5′ end with biotin for surface attachment. The duplex was immobilized on a PEG-treated surface and visualized by TIRF microscopy by using the same excitation intensity used for the Rev-RRE system. The total number of fluorescent molecules visible in the field of view was monitored over time, and the resulting time course was fitted with an exponential function to determine the rate of dye photobleaching, k_{pb}.

ACKNOWLEDGMENTS. We thank Prof. James Williamson (Scripps Research Institute) for insightful discussions, Elizabeth Kompfner for assistance with Rev mutagenesis and expression, and Goran Pljevaljcic for help in preparing the figures. This work was supported by National Institutes of Health Grants PO1 GM66669 and P50 GM082545 and the National Science Foundation Graduate Research Fellowship (W.R.).

1. Pollard VW, Malim MH (1998) The HIV-1 Rev protein. *Annu Rev Microbiol* 52:491–532.
2. Daly TJ, Cook KS, Gray GS, Maione TE, Rusche JR (1989) Specific binding of HIV-1 recombinant Rev protein to the Rev-responsive element in vitro. *Nature* 342:816–819.
3. Daly TJ, *et al.* (1993) Biochemical characterization of binding multiple HIV-1 Rev monomeric proteins to the Rev responsive element. *Biochemistry* 32:10497–10505.
4. Mann DA, *et al.* (1994) A molecular rheostat: Co-operative Rev binding to stem I of the Rev response element modulates human immunodeficiency type-1 late gene expression. *J Mol Biol* 241:193–207.
5. Malim MH, Bohnlein S, Hauber J, Cullen BR (1989) Functional dissection of the HIV-1 Rev *trans*-activator-derivation of a *trans*-dominant repressor of Rev function. *Cell* 58:205–214.
6. Malim MH, Cullen BR (1991) HIV-1 structural gene expression requires the binding of multiple Rev monomers to the viral RRE: Implications for HIV-1 latency. *Cell* 65:241–248.
7. Cook KS, *et al.* (1991) Characterization of HIV-1 Rev protein: Binding stoichiometry and minimal RNA substrate. *Nucleic Acids Res* 19:1577–1583.
8. Zapp ML, Hope TJ, Parslow TG, Green MR (1991) Oligomerization and RNA binding domains of the type 1 human immunodeficiency virus Rev protein: A dual function for an arginine-rich binding motif. *Proc Natl Acad Sci USA* 88:7734–7738.
9. Olsen HS, Cochrane AW, Dillon PJ, Nalin CM, Rosen CA (1990) Interaction of the human immunodeficiency virus type 1 Rev protein with a structured region in env mRNA is dependent on multimer formation mediated through a basic stretch of amino acids. *Genes Dev* 4:1357–1364.
10. Cole JL, Gehman JD, Shafer JA, Kuo LC (1993) Solution oligomerization of the rev protein of HIV-1: Implications for function. *Biochemistry* 32:11769–11775.
11. Axelrod D (1989) Total internal reflection fluorescence microscopy. *Methods Cell Biol* 30:245–270.
12. Ha T, *et al.* (2002) Initiation and re-initiation of DNA unwinding by the Escherichia coli Rep helicase. *Nature* 419:638–641.
13. Edgcomb SP, *et al.* (2008) Protein structure and oligomerization are important for the formation of export-competent HIV-1 Rev-RRE complexes. *Protein Sci* 17:420–430.
14. Gabdoulline RR, Wade RC (2002) Biomolecular diffusional association. *Curr Opin Struct Biol* 12:204–213.
15. Heaphy S, *et al.* (1990) HIV-1 regulator of virion expression (Rev) protein binds to an RNA stem-loop structure located within the Rev response element region. *Cell* 60:685–693.
16. Kjems J, Brown M, Chang DD, Sharp PA (1991) Structural analysis of the interaction between the human immunodeficiency virus Rev protein and the Rev response element. *Proc Natl Acad Sci USA* 88:683–687.
17. Jain C, Belasco JG (2001) Structural model for the cooperative assembly of HIV-1 Rev multimers on the RRE as deduced from analysis of assembly-defective mutants. *Mol Cell* 7:603–614.
18. Sheinerman FB, Norel R, Honig B (2000) Electrostatic aspects of protein-protein interactions. *Curr Opin Struct Biol* 10:153–159.
19. Van Ryk DI, Venkatesan S (1999) Real-time kinetics of HIV-1 Rev-Rev response element interactions. Definition of minimal binding sites on RNA and protein and stoichiometric analysis. *J Biol Chem* 274:17452–17463.
20. Nelville M, Sutz F, Lee L, Davis LI, Rosbash M (1997) The importin beta family member Crm1p bridges the interaction between Rev and the nuclear pore complex during nuclear export. *Curr Biol* 7:767–775.
21. Fang J, *et al* (2004) A DEAD box protein facilitates HIV-1 replication as a cellular co-factor of Rev. *Virology* 330:471–480.
22. McKinney SA, Joo C, Ha T (2006) Analysis of single-molecule FRET trajectories using hidden Markov modeling. *Biophys J* 91:1941–1951.